# Impact Fracture of Screws for Disassembly

D. Studny

D. Rittel*
Mem ASME

E. Zussman*
Assoc Mem ASME

Faculty of Mechanical Engineering,
Technion—Israel Institute of Technology,
Haifa 32000, Israel

*Environmental legislation urges manufacturers to develop effective technologies to cope with obsolete products. The goal is to optimize the disassembly procedure (cost, efficiency) with emphasis on potential recycling. In this work we adopt a destructive approach to product disassembly as an alternative to reverse assembly. Specifically we investigate unsupported screwed assemblies for which the screw head is protruding. Disassembly consist of breaking this head by applying side impact. The transient forces are measured by means of an instrumented bar. Experiments were conducted on various screw diameters and materials to assess the feasibility of this process. Typical design parameters (energy, time and forces) were measured. The fracture mechanism(s) was characterized by fractographic analysis. Results are presented and potential applications of this technique to efficient disassembly are discussed. The results are integrated into the preliminary design of robotic disassembler.*

## 1 Introduction

Environmental issues are becoming increasingly important for product designers and manufacturers. Public awareness of the value and fragility of an intact ecology is constantly growing, and the traditional assumption that the cost of ecological burdens should be shared by the society as a whole is no longer accepted. The European Union, for example, has introduced a set of guidelines: the Eco-Management-and-Audit Scheme (EMAS). Although still voluntary, EMAS signals that environmental responsibility lies with industry. In Germany, for instance, this attitude is already being enforced with legislation guided by the take back principle (Alting, 1995).

This trend is most apparent in the case of worn-out products. Shortage of dumping sites and waste-incineration facilities constantly remind us that products do not merely disappear after disposal. While it is widely acknowledged that the most ecologically sound approach to worn-out products is recycling, it is rarely possible or beneficial to recycle a product completely. The aim is to maximize recycled resources and minimize possible damage by the remainder that is dumped, while considering economic factors as well as other side-effects.

The natural solution is product disassembly which can lead to cost minimization, hazardous materials isolation, and opportunities to re-use or re-utilize materials and components. However, unlike traditional manufacturing processes which are based on dedicated assembly line per product, disassembly processes are characterized by a high variety of products (similar but not identical), manufacturers and uncertainty in product condition or integrity after usage. Therefore, an appropriate disassembly technology must combine flexibility and robustness to be able to deal with products with these issues. There are two approaches for disassembly:

(a) Follow the inverse problem of an assembly operation (which can be denoted as a nondestructive disassembly).
(b) Use destructive methods and cut product parts and joining elements in an irreversible way.

In this research we follow the destructive approach and aim at developing a robust approach for separating joining elements such as screws. The destructive approaches that can be found in the literature are mainly used in the recycling process for fast and efficient separation of products. Hanft and Kroll (1995) deal with classification of disassembly operations utilizing different approaches such as: drilling sawing, grinding and proposed a metric for evaluation. Seliger et al. (1995) presented a method, based on two stages: first create an acting interface on the joining elements and then use conventional assembly tools in order to loosen the joining element. Feldmann et al. (1995) proposed to combine transmission of torque with drilling.

In contrast to the above mentioned approaches we propose to apply the destructive disassembly procedure based on (single point) impact mechanics (used in the context of dynamic fracture by Giovanola (1986)). Here the joining element (screw fastener) is subjected to lateral impact on its head, when accessible, or nut, for protruding nut-secured screws. Local deformation and fracture follow impact as a result of inertia solely. In other words, the screw and the rest of the product are neither supported nor constrained by an additional *ad-hoc* fixture. The present research comprises not only a feasibility study but also qualitative and quantitative results which may provide the guidelines for practical future applications. Keeping the practical application in mind we limit ourselves to screw-joints protruding from the surfaces they are joining. *Protruding is essential for the applicability of universal lateral impact hammer for all fastening screws within our application.*

The paper is organized as follows: after the introduction we describe, in section 2, the general framework: experimental setup, theory and calibration procedure. Then the experimental results are presented in section 3, describing the calibrating parameters, analyzed test results and scanning electron fractographic analysis. Finally we discuss the results and their interpretation, addressing potential applications of this technique along with its integration into a robotic arm.

## 2 General Framework

A detailed description of the experimental set up is given in this section along with the theoretical framework which is the base of this work. Calibration was the first measurement stage followed by actual test measurements.

**2.1 Experimental Setup.** The general philosophy is to use an "instrumented bar" (Kolsky, 1963) to apply and measure transient loads. Preliminary testing was conducted on a "Split Hopkinson Bar" test fixture (Kolsky, 1963). This kind of test is commonly used to apply and measure transient loads to cylindrical specimens inserted between the bars. Here the

* Corresponding authors: merittel@techunix.technion.ac.il; eyal@hitech.technion.ac.il

Contributed by the Manufacturing Engineering Division for publication in the JOURNAL OF MANUFACTURING SCIENCE AND ENGINEERING. Manuscript received Sept. 1996; revised May 1997. Associate Technical Editor: T. C. Woo.

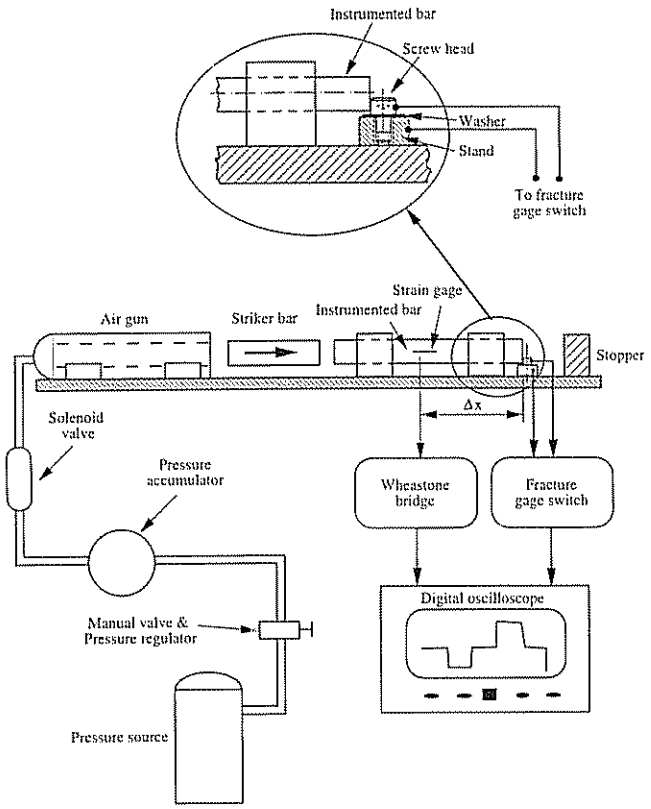


**Fig. 1 Side impact test and data acquisition apparatus, based on an instrumented bar**

screw-head was sandwiched between the two bars (incident & transmitter) and the energy input into the fracture process could be evaluated from energy balance considerations.

However, tests conducted this way showed that the "transmitter bar" (i.e. the one that receives the transferred energy) causes the screw-head to "smash" without detaching from screw body, meaning that energy was mostly invested into plastic deformation. In a subsequent series of experiments, we adopted the single instrumented bar configuration as a means to apply and measure the transient loads. This side-impact apparatus (Fig. 1) proved to be quite efficient to fracture the screw heads. The screw head is brought into contact with a high strength steel bar (12.7 mm dia) on which strain gages have been cemented at its midlength (instrumented – bar). This bar is impacted by a striker launched by an air gun at velocities ranging from 10–60 m/s (for these tests we used velocities at the range of 10–30 m/s). In this setup two stress waves are generated: the incident stress wave ($\epsilon_{inc}$) generated by the striker's impact and the reflected stress wave ($\epsilon_{ref}$) formed by the reflection of the pulse at the screw-head/bar interface. The typical pulse duration varies with the length of the striker and in our experiments this length was 0.17 m so that the pulse duration was 66 $\mu$s. Fracture of the screw's head is detected through the interruption of an electrical circuit (fast rising gate). The screw is inserted in series into the electrical circuit. With this fracture switch we determined the exact time at which the screw head was totally detached of the body of the screw. Sampling of the pulses was achieved using a digital oscilloscope (Nicollet 490) at a sampling rate of 5 MHz.

During the whole process, the screw-stand is unsupported, so fracture occurs due to the inertia of the screw-stand assembly as a counter force to the impact. The recorded signals can be converted into interfacial (bar to screw-head) displacement and force pulses, as shown next.

**2.2 Theoretical Test Analysis.** (Kolsky, 1963; Johnson, 1983; Zukas, 1963) The stress, strain and striker-velocity relations are given by:

$$\sigma_{in} = E\epsilon_{inc} = \tfrac{1}{2}\rho C_L V_{striker} \quad (1)$$

where:

$\sigma_{in}$ = input stress wave in the instrumented bar
$E$ = Young's Modulus of the instrumented bar
$\epsilon_{inc}$ = incident strain wave in the instrumented bar
$\rho$ = density of the instrumented bar
$C_L$ = longitudinal wave velocity in the instrumented bar
$V_{striker}$ = striker velocity

The interfacial velocity $V_1$ is given by: (at the screw-head to bar interface):

$$V_1 = C_L(\epsilon_{inc} - \epsilon_{ref}) \quad (2)$$

where: $\epsilon_{ref}$ = reflected strain wave in the instrumented bar
The interfacial force $F_1$ is given by:

$$F_1 = EA(\epsilon_{inc} + \epsilon_{ref}) \quad (3)$$

where: $A$ = cross section area of the instrumented bar
The "energy loss" in the instrumented-bar, equals the energy transferred to the screw-head (creating fracture of screw head) The balance of energy writes as:

$$U_{screw} = U_{inc} - U_{ref} \quad (4)$$

Where $U_{inc}$ and $U_{ref}$ stand for the incident and reflected energy respectively and $U_{screw}$ is the energy invested in the screw. which in terms of the incident and reflected pulses becomes:

$$U_{screw} = AC_L E \int_{t1}^{t2} (\epsilon_{inc}^2 - \epsilon_{ref}^2) d\theta \quad (5)$$

where $\theta$ varies from: $t1$—the beginning of the stress pulse (10% rise)
to: $t2$—the fracture gage pulse (fracture time).
The over-all fracture energy $U_{screw}$, is the basic parameter required for future design of fracture apparatus for fast disassembly of screw fasteners. Of course, its accurate evaluation relies on the accurate determination of $\epsilon_{inc}$ and $\epsilon_{ref}$.

**2.3 Calibration Procedure.** Two important factors affect the results accuracy. The first is related to the dispersion and attenuation of the pulses in the bar and the procedures employed to account for these phenomena (Kolsky, 1963; Lifshitz, 1994). The second factor is related to the nature of the contact between the instrumented bar and the screw head which causes a high level of reflected pulse. In these experiments, by contrast with "classical impact tests," the contact area between the bar and the screw head is poorly defined as it is closer to a line than to a plane. The level of reflection is thus quite high due to the mismatch of mechanical impedance. Since the fracture energy relies, among other things, on the sum of two signals [incident and reflected, see Eq. (5)] which are very similar but of opposite sign, one has to ensure that the measurement does not reflect merely "background noise" (this issue was addressed in another context by Maigre and Rittel, 1995). Ideally, for a free-end bar the incident and reflected pulses should be identical, provided the pulses are corrected for geometrical dispersion. In other words, after correction the net interfacial force should be zero (free end condition) and the dissipated energy should be zero as well. Consequently, the first step was to calibrate the system on a series of free-ended bar experiments, by:

i. Correcting the pulses in view of the geometric dispersion.
ii. Determining the average linear attenuation coefficient of the signal (damping).

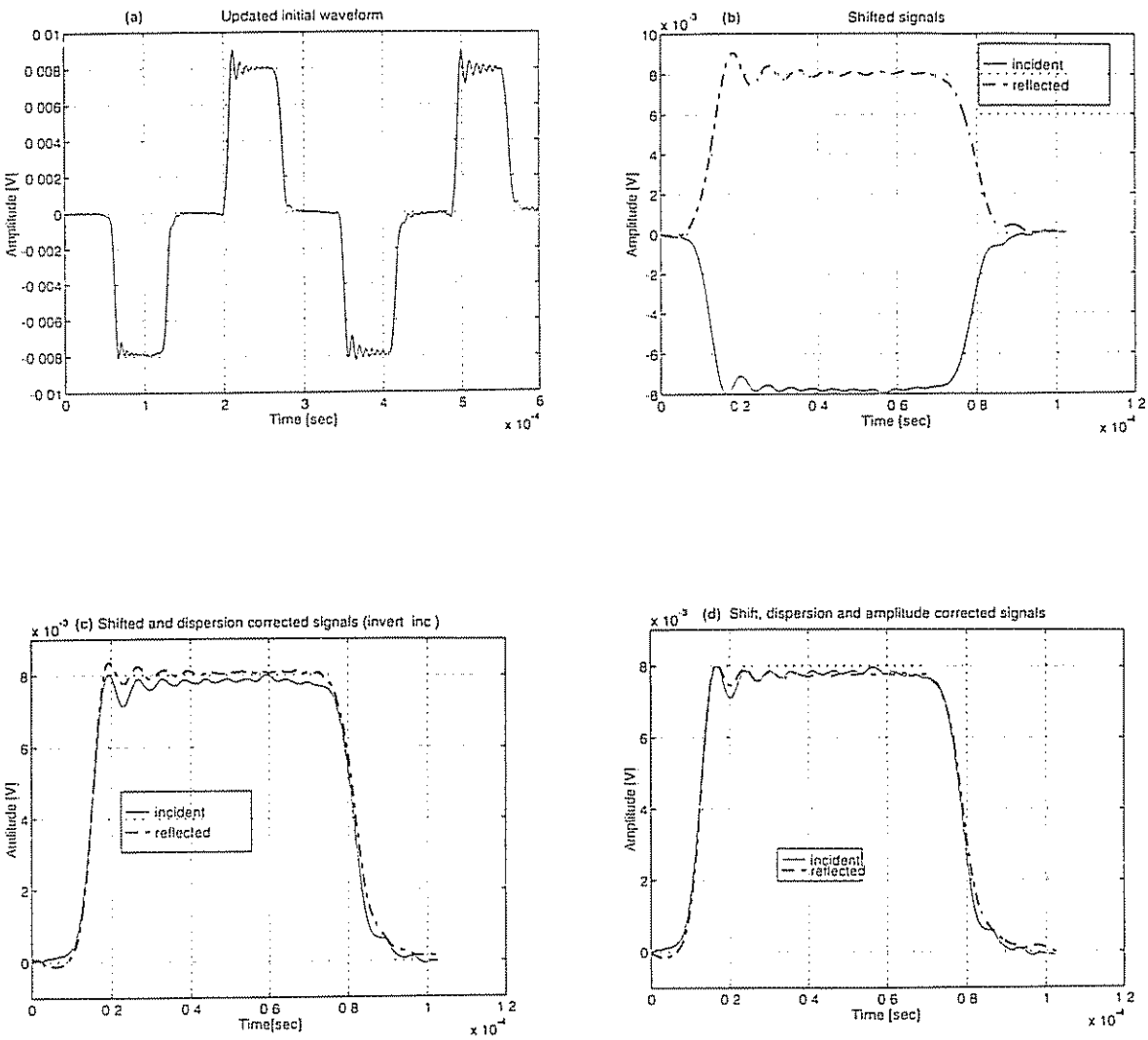


**Fig. 2 Typical 'Free-End' test results: (*a*) initial wave form (incident pulse – compression, reflected pulse – tension) (*b*) first incident pulse shifted to the reflected pulse (c) dispersion corrected pulses (with inverted incident) (*d*) reflected and inverted incident pulses, after damping correction (residual energy: 9.2E-3[J])**

Linear attenuation is generally not accounted for, when geometrical dispersion corrections are carried out. We included this *ad-hoc* correction to improve the quality of the signal corrections as addressed next. The damping factor is given by:

$$I_c = I_0 * \exp(-\alpha * \Delta x) \tag{6}$$

Where:

$\alpha$ = damping factor
$\Delta X$ = distance traveled by the pulse along the bar
$I_0$ = the initial pulse's amplitude
$I_c$ = the corrected pulse's amplitude

The corrections were performed using signals, from a free-end bar tests. The incident pulse was first shifted forward in time to coincide with the first reflected pulse. The forward time shifted incident pulse was corrected for geometric dispersion. Then, we compared the amplitudes of the forward time shifted incident pulse and the first reflected pulse as recorded, and calculated the average ratio $(I_c/I_0)$. Then the damping factor was calculated according to Eq. (6).

The experimental pulses were subsequently corrected using the dispersion corrections along with this damping factor. Care was paid to the sign of the correction (positive or negative damping factor) according to the shifting, forward or backward in time (which correlates with space) of the signal, with respect to screw-head/bar interface.

## 3 Experimental Results

This paragraph details all experimental results following those stages: calibration tests—numerical and graphical results of actual fracturing tests—macro and micro fractographic observations and conclusions.

**3.1 Calibration.** Conducting and averaging a series of 12 "free end" experiments (typically represented in Fig. 2(*a*) to 2(*c*)) we found the following average damping factor:

$$\bar{\alpha} = -0.050 \pm 0.009$$

Calculation of the energy loss in the instrumented bar after applying all necessary corrections (dispersion, damping) should ideally be equal to zero for these free-end bar tests. From the same series of experiments it was found that the average energy is indeed very small but not negligible *a-priori* [applying Eq. (5) to Fig. 2(*d*)] with the following value:

$$\bar{U} = 0.0075 \text{ [J]} \pm 0.0041 \text{ [J]}$$

This value was systematically subtracted from all subsequent

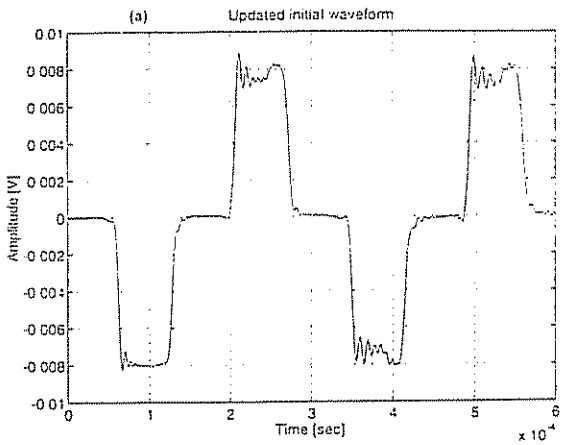


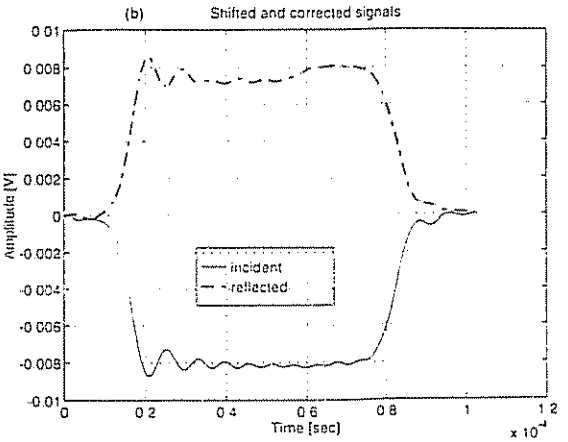


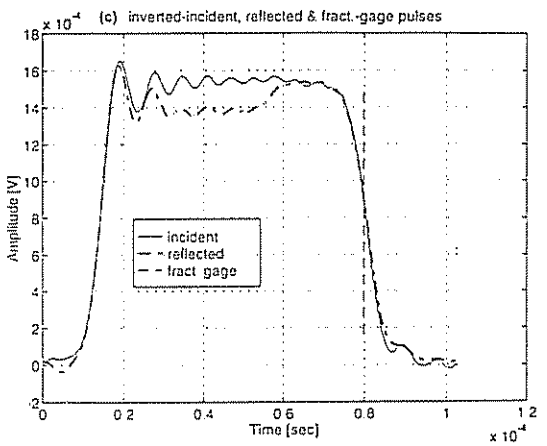


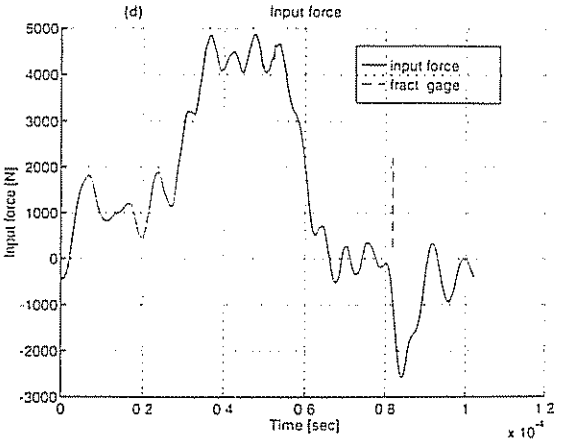


**Fig. 3 Typical test results for M3 carbon steel screw: (*a*) initial wave form (incident pulse – compression, reflected pulse – tension) (*b*) first incident and reflected pulses shifted to the interfacial plane with dispersion and damping corrected (*c*) $\epsilon_{ref}$ and inverted $\epsilon_{inc}$ along with fracture pulse ($U_{screw}$ = 2.11[J]) (*d*) interfacial force (equivalent to: $\epsilon_{inc} + \epsilon_{ref}$) along with fracture pulse**

values obtained in actual tests as an estimate of the average error.

**3.2 Test Results.** The experiments were conducted on commercial stainless steel and carbon steel screws with diameters ranging from 2.0 to 5.0 mm. These screws are the most commonly used, e.g., in standard commercial electronic systems. All screws fractured subsequent to impact.

A typical sequence of the recorded and analyzed pulses is shown in Fig. 3 (M3 carbon steel screw). The raw pulses are shown in Fig. 3(*a*). The incident and the first reflected pulse are shown next in Fig. 3(*b*) after shifting both of them to the screw-head/bar interface plane and after the correction process (dispersion and damping corrected). A feature, which is common to all tests, is that the reflected pulse overlaps with the incident pulse after a certain amount of time (typically 60 $\mu$s) within the first reflected pulse duration, as shown in Fig. 3(*c*), so that the difference between the two pulses is merely zero from the merging point and further on. The fracture switch, on the other hand, signals fracture on an average of 15 $\mu$s later. Figure 3(*d*) shows the interfacial force which is derived from the sum ($\epsilon_{inc} + \epsilon_{ref}$). The experimental results are summarized in Table 1.

**Table 1*a* Test results of carbon-steel screws**

| screw type | core diameter [mm] | number of tests | striker velocity [m/sec] | input force [$10^3$*N] | fracture energy [J] |
|---|---|---|---|---|---|
| M2.0 X 0.4 | 1.57 | 3 | 15.5 - 16.1 | 2.0 - 2.3 | 0.55 - 0.88 |
| M2.5 X 0.45 | 2.01 | 9 | 15.8 - 16.5 | 2.7 - 3.1 | 0.70 - 1.16 |
| M3.0 X 0.5 | 2.34 | 6 | 15.5 - 16.2 | 4.5 - 5.2 | 1.86 - 3.14 |
| M4.0 X 0.7 | 3.09 | 7 | 19.5 - 20.5 | 7.2 - 8.8 | 4.94 - 6.17 |

**Table 1*b* Test results of stainless-steel screws**

| screw type | core diameter [mm] | number of tests | striker velocity [m/sec] | input force [$10^3$*N] | fracture energy [J] |
|---|---|---|---|---|---|
| #2-56-UNC | 1.62 | 11 | 14.5 - 15.5 | 2.0 - 2.2 | 0.60 - 0.94 |
| M3.0 X 0.5 | 2.34 | 6 | 16.0 - 19.0 | 4.0 - 4.5 | 2.01 - 2.35 |
| M4.0 X 0.7 | 3.09 | 8 | 18.0 - 19.0 | 5.4 - 6.2 | 3.61 - 4.44 |
| M5.0 X 0.8 | 3.97 | 5 | 23.0 | 7.9 - 8.2 | 7.51 - 8.52 |

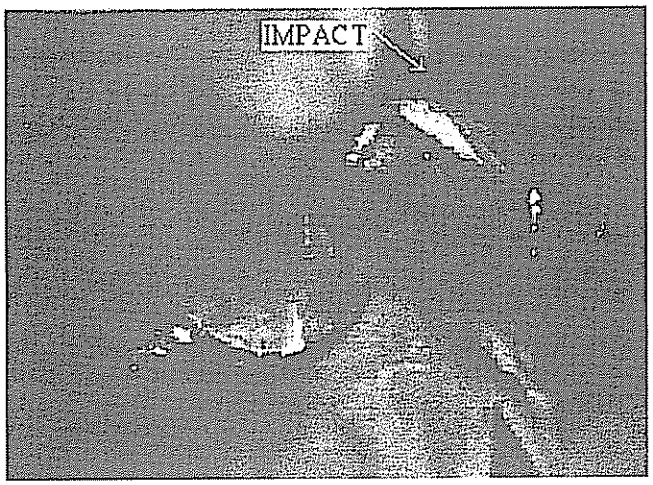


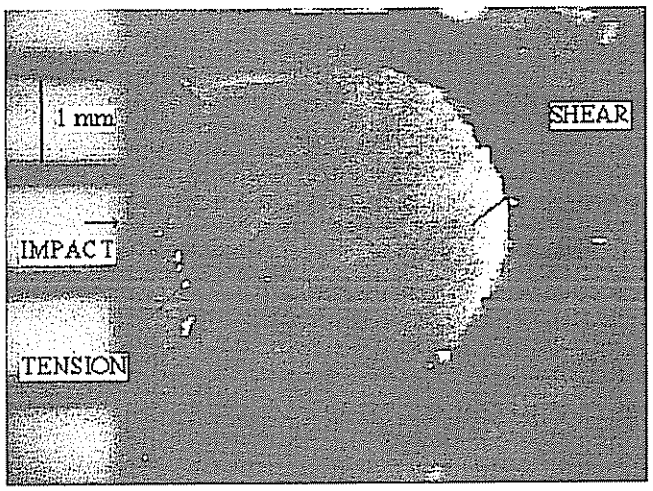


Fig. 4 Typically fractured M4 carbon steel screw

**3.3 Fractographic Results.** Macro-photographs of a typical broken carbon steel screw is shown in Fig. 4. Fracture always starts at the thread-root, with a small lip at the stress wave entrance side. The same features were observed regardless of the investigated material or screw diameter.

Typical scanning electron fractographs are shown in Fig. 5. These fractographs show characteristic **ductile fracture** micro-mechanisms, caused by joint shear and tensile mechanisms. Tensile ductile failure is evidenced at the stress wave entrance side (equi-axed dimples) followed immediately by ductile shear (U-shaped) dimples (Metals Handbook, 1974). As one progresses away from the side of the impact the area fraction of shear dimples increases.

## 4 Discussion

Several important points related to the experiments will now be addressed, keeping in mind the "design for disassembly" aspects of this work.

Time to fracture is important since it sets the upper limit on time for the integral leading to the overall energy invested in the screw. Since there is a clear difference of about 15 $\mu$s between the time at which the pulses overlap (free end condition) and the time indicated by the fracture switch, one might wonder which of these two readings is more accurate. On the one hand, pulses overlap means that contact is lost (or very poor) between the bar and the screw head. On the other hand the fracture switch indicates total fracture of the screw, so that one might tentatively interpret these 15 $\mu$s as some characteristic time scale of the fracture process itself (crack propagation phase). At any rate the increment of energy is negligible between either of these time limits. For the sake of consistency, all the calculations of energy reported here have been based on the readings of the fracture switch.

The next point concerns the nature of the energy invested in the screw. It should be emphasized that energy here includes the deformation, fracture and kinetic energy terms all at once. Since we cannot separate the total energy into its individual components, we can just assume that the dominant term is that related to deformation and fracture. The measurements reported here are quite similar to Charpy or Izod tests (Hertzberg, 1989) carried out routinely to characterize materials resistance to impact loading. In these tests too, the energy is measured under the same assumptions. We observed that all fractures were of a ductile character (by mixed tension and shear). This assigns a character of *upper shelf fracture* behavior when comparing

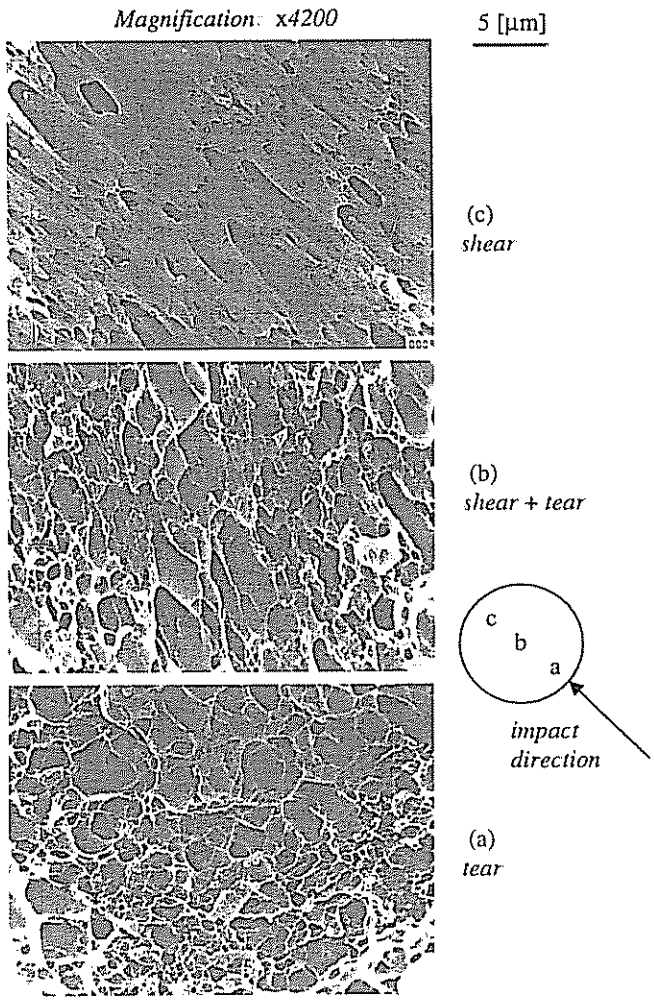


Fig. 5 Typical SEM phractographs of fractured M4 carbon steel screw head: (*a*) at the impact entrance side (*b*) at the center of fractured area (*c*) opposite to the impact side

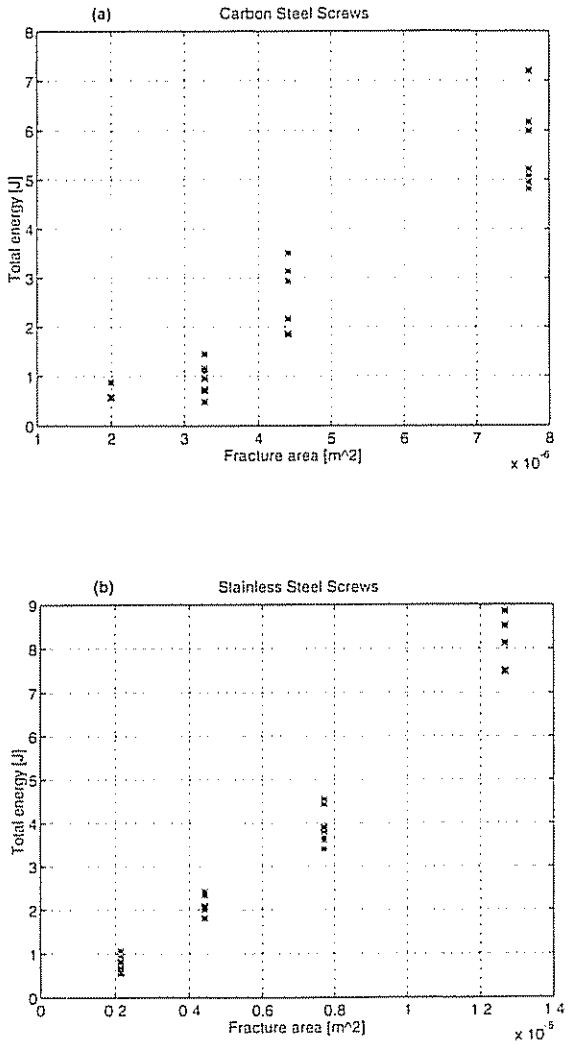


**Fig. 6 Total fracture energy vs. net fracture area: (*a*) carbon steel screws (*b*) stainless steel screws**

these results to tests such as Charpy or Izod. This is to be contrasted with other types of screws which would fail in a brittle manner, thus requiring smaller total energies. This upper bound is of importance to the future design of a disassembly machine.

We did not attempt to "improve" our waveguide (incident bar) by shaping its end into a chisel type profile. Preliminary experiments with such profiles were carried out which yielded highly distorted stress waves, thus useless for our quantitative purposes exposed in this paper. Nevertheless, the screw heads fractured so that it is reasonable to assume that the shape of the impacting end can be modified with respect to the present one.

Another important point is that of the angle of impact. In our work, we only consider impact perpendicular to the screw head which is obviously the most efficient way to shear it off. Practical situations might involve different angles whose influence remains to be assessed.

To gain further understanding of the process, it seems natural to normalize the total energy by dividing it by the net fracture area as shown in Fig. 6. This figure shows that this ratio is not constant as expected, e.g., in a Charpy test, neither for stainless nor for the carbon steel screws. Rather, a power dependence of the energy on the net fracture area is noted. Keeping in mind that failure always starts at the thread root, it seems natural to introduce this geometrical parameter of the screw into the relation, as shown next.

Early work on fracture mechanics showed a similar dependence between the static stress intensity factor (more precisely, the plane strain fracture toughness $K_{Ic}$) and the square root of the notch root radius $\sqrt{\rho}$ in Charpy specimens (Malkin and Tetelman (1971), as well as Swanson (1986)):

$$K_{Ic} \propto \sqrt{\rho} \tag{7}$$

This relation is very similar to the one observed here between the overall energy and $\sqrt{\rho}$. It is also known that the energy release rate $G$ can be correlated to the stress intensity factor(s) $K$ (I, II or their combination) (Hertzberg, 1989):

$$G \propto \frac{K^2}{E} \tag{8}$$

Therefore, $G$ and $K$ are related to $\sqrt{\rho}$ (Swanson, 1986; Hertzberg, 1989).

Consequently, when *dynamic fracture* is considered, one naturally attempts to correlate a representative energy release rate to the dynamic stress intensity factor(s). Several empirical correlation were proposed in this spirit to assess the dynamic stress intensity factor $K_{Id}$ (Hertzberg, 1989). Such correlation relate $K_{Id}$ to the Charpy V-notch energy: $G_{CVN}$ and they generally write as (Hertzberg, 1989; Nageswara and Acharya, 1992):

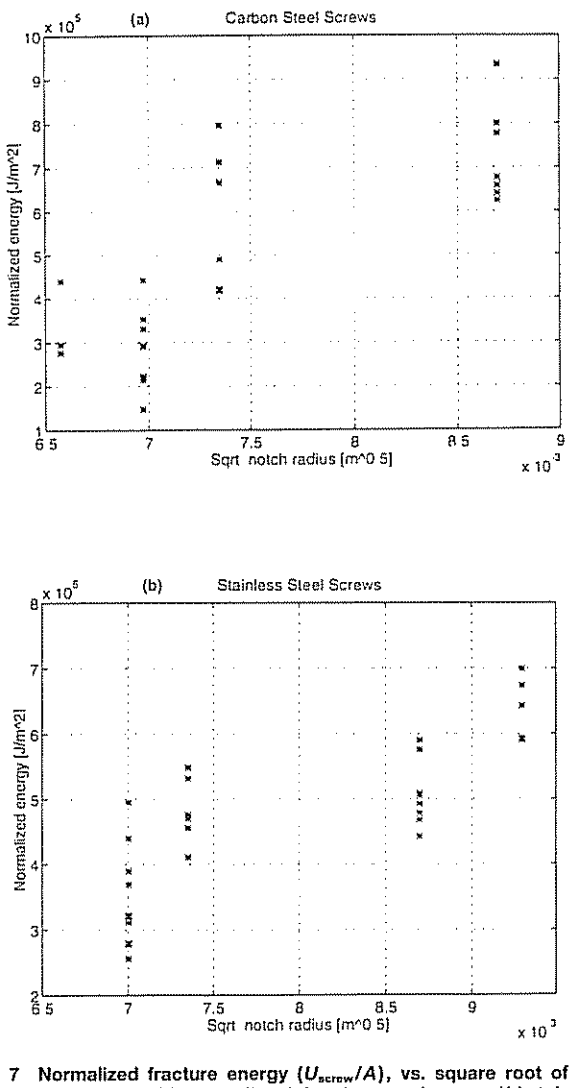


**Fig. 7 Normalized fracture energy ($U_{screw}/A$), vs. square root of the standard thread (notch) root radius: (*a*) carbon steel screws (*b*) stainless steel screws**

$$G_{CVN} \propto \frac{K_d^2}{E} \tag{9}$$

In our work we assimilate $U_{screw}$ to $G_{CVN}$ so that one expects that $U_{screw}$ like $K_d$ be related to $\sqrt{\rho}$ as well.

Consequently, we now replot the normalized $U_{screw}$ as function of the square root of the thread root radius $\sqrt{\rho}$. The thread root radius can be assessed from manufacturing standards for screws (ISO, 1984) as follows:

$$\text{ISO standard where} \quad \rho \cong 0.108 * P$$

$$\text{UNIFIED standard where} \quad \rho \cong 0.142 * P$$

Where $P$ is the screw pitch.

Figure 7 shows this relation and it can be noted that several points (or group of points) *do not lie* on the expected curve while deviation is mostly apparent for the carbon steel screws compared to the stainless steel screws.

To account for this discrepancy, we checked the screw's tooth geometry using optical comparator. Figure 8 is a plot of the measured vs. expected root radius. This figure shows large deviations from standard requirements mostly in the carbon steel screws.

Figure 7 can now be replotted using actual values of the thread root radius, as shown in Fig. 9. This figure shows that the points now lie along the kind of curve predicted by the empirical fracture mechanics model, thus allowing to properly take into account the thread root geometry of the screws.

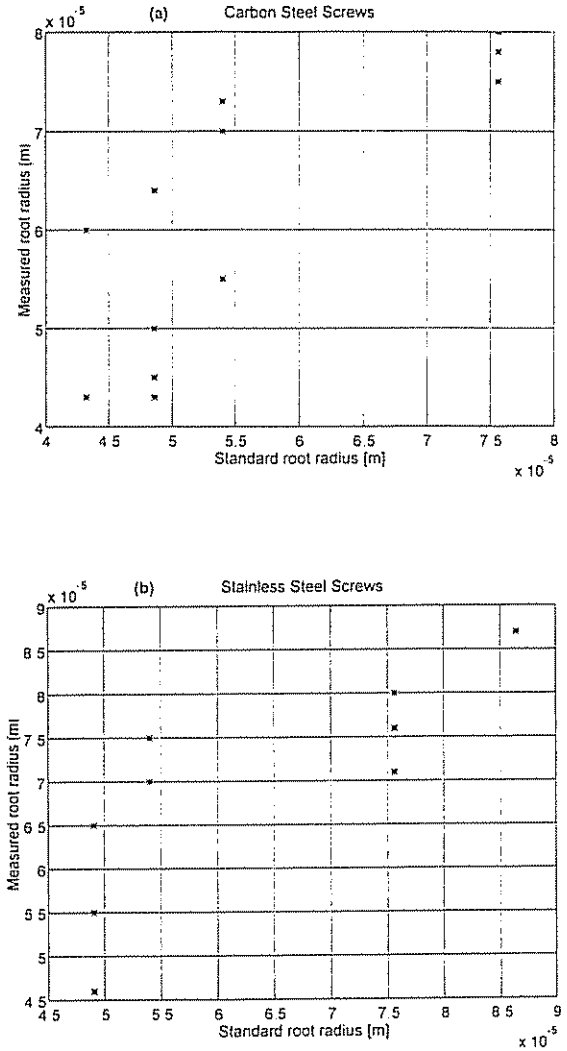


**Fig. 8 Measured thread root radiuses vs. ideal ISO and UNIFIED standards: (*a*) carbon steel screws (*b*) stainless steel screws**

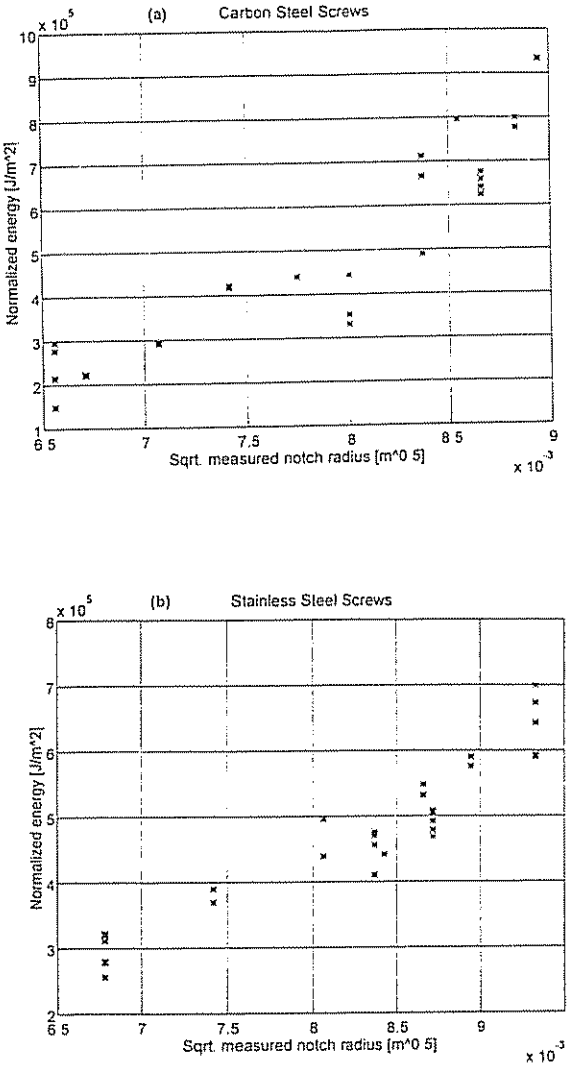


**Fig. 9 Normalized fracture energy ($U_{screw}/A$), vs. square root of the measured thread (notch) root radius: (*a*) carbon steel screws (*b*) stainless steel screws**

The reported experiments were conducted in an attempt to evaluate the feasibility and effectiveness of unsupported "as is," vs. supported assembly, and we found out that dynamic fracture of unsupported screw-assembly is feasible. This adds to the versatility of our approach as to the requirement for supporting the body in-work. Furthermore, the results may be useful for design purposes of a disassembly device when actual maximum values of energy, force and striker speed required for this process are given per screw material and size. The next stage is thus to implement the above mentioned results into a disassembly device.

## 5 Practical Application: Destructive Disassembler

A destructive disassembly device had been designed for practical applications, based on the above analysis (Fig. 10). The device's sizes and weight are constrained to a medium size robotic arm, which limits us to max. sizes of 300 × 200 × 200 mm and max. weight of 10 kg. Electro-pneumatic system activates and controls the device, while electro-optical vision system is assisting in accurate positioning of the active edge (this feature is beyond the scope of this work).

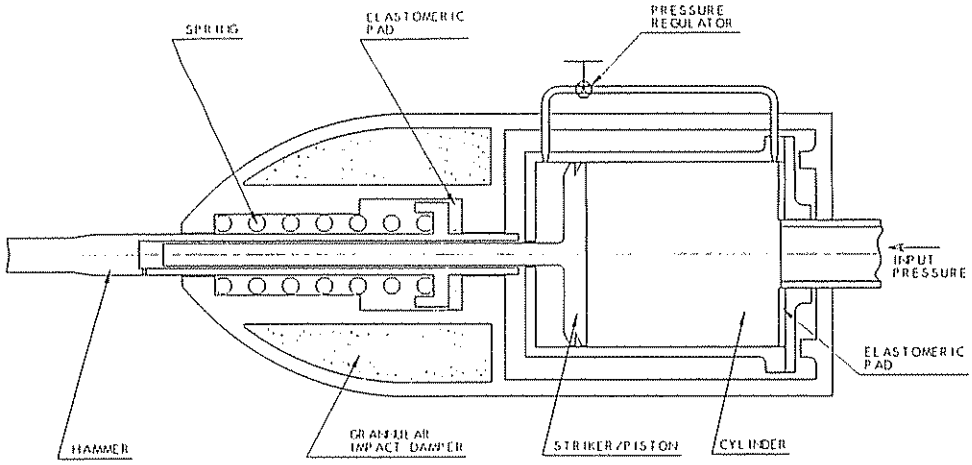


**Fig. 10 Layout of the developed destructive disassembly apparatus**

A high strength/hardness steel hammer treated for optimal toughness will be in contact with screw head, where the interface surface is shaped to have the best contact surface at +10°, in order to improve accessibility and minimize parasitic forces that might develop due to misalignments. The striker, made of hardened stainless steel, is pneumatically driven with a 10 Atm pressure line that can be regulated with respect to a given fastener. The supplied pneumatic pressure to the striker is stabilized during the acceleration period, by a pressure vessel, acting as a "pressure battery." Electro-pneumatic control system regulates the pressure-pulse duration for accelerating the striker, as well as the backward movement of the striker and hammer. Since impacts created by this process are significantly high (up to $10^3$ N) and short (40 $\mu$sec), a granular impact damper was integrated in the disassembler.

Disassembler design considers various geometric constraints and the required dynamic effects. Striker mass should be at least 0.2 Kg and a maximum required velocity of 25 m/sec. These requirements guarantee fracture of screws and fasteners with characteristics similar to those tested.

The significant design parameters are the piston's stroke and diameter. The orifice's diameter is limited due to the required set-up on the robotic arm. In our case the maximal value of the orifice's diameter is 12.7 mm.

The physical relations describing the dynamic process of filling in the piston's volume are as follow (Din, 1956; Hatsopoulos and Keenan, 1965; Shaanan, 1969):

$$\text{The mass flow:} \quad G^{\&} = \frac{A \cdot C_2 \cdot C_d \cdot P_u \cdot F}{\sqrt{T}} \tag{10}$$

$$\text{The acting force:} \quad F = f \cdot \left(\frac{P_d}{P_u}\right) = \frac{C_1}{C_2} \cdot \left(\frac{P_d}{P_u}\right)^{1/k} \cdot \sqrt{1 - \left(\frac{P_d}{P_u}\right)^{k-1/k}} \quad P_d \geq P_{cr} \tag{11}$$

Where:

$$C_1 = \sqrt{\frac{2 \cdot k}{(k-1) \cdot R}} \quad \left[\frac{\sec \sqrt{^\circ\mathrm{K}}}{\mathrm{m}}\right]$$

$$C_2 = \sqrt{\frac{k}{R \cdot \left(\frac{k+1}{2}\right)^{k+1/k-1}}} \quad \left[\frac{\sec \sqrt{^\circ\mathrm{K}}}{\mathrm{m}}\right]$$

$$P_{cr} = P_u \cdot \left(\frac{2}{k+1}\right)^{k/k-1} \quad \left[\frac{\mathrm{N}}{\mathrm{m}^2}\right]$$

$A$ [m$^2$] Orifice area

$G^{\&}$ $\left[\frac{\mathrm{Kgm}}{\sec}\right]$ Mass flow

$P_u, P_d$ $\left[\frac{\mathrm{N}}{\mathrm{m}^2}\right]$ Pressure before and after the orifice respectively

$T$ [°K] Temperature

$R$ $\left[\frac{\mathrm{N \cdot m}}{\mathrm{Kg \cdot {}^\circ K}}\right]$ Specific gas constant

$C_p$ $\left[\frac{\mathrm{m}^2}{\sec^2 \cdot {}^\circ\mathrm{K}}\right]$ Specific heat at constant pressure

$C_v$ $\left[\frac{\mathrm{m}^2}{\sec^2 \cdot {}^\circ\mathrm{K}}\right]$ Specific heat at constant volume

$C_d$ (non dimensional) Orifice quality constant between 1:0

$k = \frac{C_p}{C_v}$ Specific heat ratio

Design is done in two iterations: first we determine the gas flow in terms of mass and volume, where the pressure in the piston is determined through the ideal gas state equation. Determining the dynamic features of the piston ends with the new cylinder free volume. Second iteration starts if we find out that the input pressure drops due to excesses increase of the cylinder free volume. In this case we force the pressure to be constant in time and we determine the cylinder new free volume from the gas state equation. The whole process is a time dependent calculation with finite time steps. The calculation is ended when the required piston's velocity is reached.

## 6 Summary

Motivated by recycling considerations we proposed in this paper a novel approach for destructive disassembly of screwed assemblies.

Dynamic fracture of screwed fasteners was proven to be feasible and is therefore applicable to rapid cost effective disassembly tools.

Increased flexibility was gained by considering unsupported assemblies.

The fracture energy and mechanisms were systematically characterized for typical screw diameters and two different materials.

A simple fracture mechanics model was used to relate the fracture energy to the screw geometrical parameters.

The present results comprise the basic parameters needed for the synthesis of the disassembler presented here.

## 7 Acknowledgments

This research has been supported in part by the Fund for the Promotion of Research at the Technion, Research No. 033-039.

## 8 References

Alting, L., 1995. "Life Cycle Engineering and Design." *Annals of the CIRP*. Vol. 44, No. 2, pp. 10–14.

Din, F., 1956. *Thermodynamic Functions of Gases*. Butterworth. London.

Feldmann, K., and Meedt, O., 1995. "Recycling and Disassembly of Electronic Devices," *Proceedings. Prolomat '95*. F-L. Krause. ed., Berlin, Germany. pp. 233–245.

Giovanola, J. H., 1986. "Investigation and Application of the One-Point-Bend Impact Test." ASTM STP 905. American Society of Testing and Materials. Philadelphia. PA. 307–328.

Hanft, T. A., and Kroll, E., 1995. "Ease of Disassembly Evaluation in Design for Recycling," *Design for X-Concurrent Engineering Imperatives*. Huang. G. Q., ed., Chapman & Hall.

Hatsopoulus, G. N., and Keenan, J. H., 1965. *Principles of General Thermodynamics*. John Wiley & Sons, New York. NY.

Hertzberg. R. W., 1989, *Deformation and Fracture Mechanics of Engineering Materials*. John Wiley & Sons, 3rd ed., New York. NY.

Johnson. W., 1983, *Impact Strength of Materials*. Edward Arnold.

Kolsky, H., 1963. *Stress Waves in Solids*. Dover Publication. 2nd ed.

Lifshitz, J. M., and Leber. H., 1994. "Data Processing in the Split Hopkinson Pressure Bar Tests," *Int. J. Impact Eng.* Vol. 15, No. 6. pp. 723–733.

Maigre. H., and Rittel. D., 1995. "Dynamic Fracture Detection Using the Force Displacement Reciprocity: Application to the Compact Compression Specimen." *Int. J. of Fracture*, No. 73, pp. 67–79.

Malkin, J., and Tetelman. A. S., 1971. "Relation Between $K_{Ic}$ and Microscopic Strength For Low Alloy Steels." *Engineering Fracture Mechanics*. Vol. 3. pp. 151–167.

Nageswara. R. B., and Acharya, A. R., 1992. "A Comparative Study on Evaluation of Fracture Toughness from Charpy V-Notch Impact Energy and Reduction-in area." *Eng. Fract. Mech.*, Vol. 41, No. 1, pp. 85–90.

Seliger. G., Hentschel. C., and Wagner. M., 1994. "Disassembly Factories for Recovery of Resources in Product and Material Cycles." *Proceedings. Prolomat '95*, F-L. Krause. ed., Berlin, Germany. pp. 58–67.

Shaanan, S., 1969. "Development of Fast, two-positions Electro-Pneumatic Valve for Control System," Msc. Thesis. Technion, Israel.

Swanson, R. E., Thompson, A. W., and Bernstein, I. M., 1986. "Effect of Notch Root Radius on Stress Intensity in Mode I and Mode III Loading." *Metallurgical Transactions*, Vol. 17A. pp. 1633–1636.

Zukas, J. A., 1963. *High Velocity Impact Dynamics*. John Wiley & Sons. New York. NY.

*Metals Handbook*, 1974, Fractography and Atlas of Fractographs. A. S. M., 8th ed., Vol. 9, Metals Park, OH.

International Organization for Standardization (ISO), 1984. *Fasteners and Screw Threads*. Vol. 18.